Available online at www.sciencedirect.com
ScienceDirect
Microporous and Mesoporous Materials 115 (2008) 261–266
MICROPOROUS AND MESOPOROUS MATERIALS
www.elsevier.com/locate/micromeso

Theoretical studies of IM-12 zeolite for acidic catalysts

Lihua Kang [a], Weiqiao Deng [b], Tao Zhang [c], Zhongmin Liu [c], Ke-Li Han [a,*]

[a] State Key Laboratory of Molecular Reaction Dynamics, Dalian Institute of Chemical Physics, Chinese Academy of Sciences, Dalian 116023, PR China
[b] Division of Chemistry and Biological Chemistry, School of Physical and Mathematical Sciences, 637617 Singapore, Singapore
[c] State Key Laboratory of Catalysis, Dalian Institute of Chemical Physics, Chinese Academy of Sciences, Dalian 116023, PR China

Received 29 December 2007; received in revised form 30 January 2008; accepted 30 January 2008
Available online 9 February 2008

Abstract

We theoretically investigate the properties of the IM-12 to address a catalyst for acidic conversion reaction of larger organic molecules. The acidic characteristics of the IM-12 are investigated by density functional theory (DFT) considering both the local density and generalized gradient approximations, LDA and GGA, respectively. Based on quantum mechanical (QM) calculation results, we find that the zeolite with Al element prefers the tetrahedral (T) sites, T4 and T6, when replacing Si in IM-12 framework. Isomorphously substituted IM-12 on the T4 and T6 sites by B, Al, and Ga is studied, respectively. Both of the sites give the Brönsted acidity order: B–IM-12 < Ga–IM-12 < Al–IM-12, which is the same as other zeolites. The calculated NH_3 adsorption energies are compared with the calculated and experimental results of H–[Al]MOR [M. Elanany, D.P. Vercauteren, M. Koyama, M. Kubo, P. Selvam, E. Broclawik, A. Miyamoto, J. Mol. Catal. A 243 (2006) 1; C. Lee, D.J. Parrillo, R.J. Gorte, W.E. Farneth, J. Am. Chem. Soc. 118 (1996) 3262]. Molecular dynamics (MD) results show that IM-12 zeolite allows the large molecules such as diisopropylbenzene (DIPB) and triisopropylbenzene (TIPB) to diffuse faster than those in MOR zeolite and IM-12 may have significant selectivity for TIPB over DIPB. We conclude that the IM-12 with Al impurity would be a good candidate for large organic molecule acidic conversion reaction.

Keywords: IM-12; Zeolite; Acidity; Density functional theory; Molecular dynamics

1. Introduction

Zeolites with pores comprised of larger than 12 tetrahedral atoms (T-atoms) are of great interest in oil industry. Especially, these kinds of zeolites can be used as acidic catalysts for large hydrocarbon molecules for which zeolites with small pores are not suitable. The first molecular sieve with extra-large-pore is VPI-5 [1], which was synthesized in 1988 (18-membered ring). Since that time numerous other extra-large-pore zeolites (ITQ-15 [2], UTD-1 [3,4], CIT-5 [5], ECR-34 [6], SSZ-53, SSZ-59 [7], OSO-1 [8], and ITQ-33 [9]) have been synthesized. However, most of them act as unidirectional pore zeolites and suffer from poor thermal and hydrothermal stability that limit their usefulness. Catalytic results have appeared that the potential of ultra-large-pore zeolites could be improved if the zeolites have multidirectional channel and the high thermal and hydrothermal stability characteristics [10].

Recently, two new zeolites, ITQ-15 [2] and IM-12 [11], have been reported and assigned the International Zeolite Association (IZA) structure code UTL. They are both the germanium-containing zeolite that contains the two-dimensional channel system with extra-large-pores by 14- and 12-channels. The unusual large-pores and systems of intersecting channels render these zeolites of being interesting in larger hydrocarbon molecules catalysis. It presents an opportunity to synthesize an acidic catalyst workable for large molecules. As for ITQ-15, Corma and coworkers [2] have succeeded in introducing active acid sites in the structure and the catalytic results show the benefit of its pore topology when compared with unidirectional pore zeolites (UTD-1). IM-12, a zeolite iso-structural to ITQ-

* Corresponding author.
E-mail address: klhan@dicp.ac.cn (K.-L. Han).

1387-1811/$ - see front matter © 2008 Elsevier Inc. All rights reserved.
doi:10.1016/j.micromeso.2008.01.042

15, displays a high thermal stability. This material has shown the ability to incorporate heteroatoms in the framework and been suggested that it may have catalytic applications as well. So a great deal of work needs to be done on the study of structural, adsorptive, and catalytic properties of IM-12 zeolite. A deeper understanding of these details will be of importance in the development of more efficient zeolite-based catalysts. In this work, we study the acidic catalyst based on IM-12 by using first principle calculations and molecular dynamics.

As we know, two factors determine the catalytic efficiency:

(1) *Acidities of zeolites.* It has been reported that the acidity of zeolite is of primacy significance for the catalytic properties and have led to numerous industrially important applications, such as catalysts and adsorbents [12,13]. The source of the Brönsted acidity in zeolites is the bridging hydroxyl group that arises from the presence of trivalent metal cation such as Al, B, and Ga, replacing Si in their structures. There are many experimental methods used for studying the acidity of several isomorphously substituted zeolites, such as the adsorption of probe molecules [14–16], infrared (IR) spectroscopy [17–19], and temperature programmed desorption (TPD) [19,20]. However, experimental methods [21] cannot distinguish between Si and Al or other metal atoms in tetrahedral sites, and this needed information could not be obtained directly from experiments. On the other hand, many studies have shown that quantum mechanical calculations can yield useful information for predicting the acidity and structures of the isomorphously substituted zeolites [22–25]. Unfortunately, no calculation is reported for IM-12 zeolite so far.

(2) *Sorbate diffusion inside zeolites.* The diffusion of sorbate molecules through the channel of zeolite is of great scientific interest due to applications in separation technology and catalysis [26]. In the previous decades, various experimental measures have been proposed, including quasi-elastic neutron scattering (QENS) [27,28] and pulsed-field gradient NMR (PFG-NMR) [29–32], to study the self-diffusivity of hydrocarbons inside zeolite pores. However, some dynamical diffusion processes of sorbate molecules in zeolites are generally very difficult or impossible to be interpreted only by experiments. On the other hand, molecular dynamics (MD) simulations have provided a number of insights into the diffusion of guest molecules in zeolites [33–35].

In this study, aiming at these two factors, we carried out two series of calculations. First, we systematically studied the incorporation of the Al atom in IM-12 zeolite to find out which sites are the preferential location and then studied the deprotonation energy (DPE) and the NH_3 adsorption energy (E_{ads}) of zeolite substituted with various heteroatoms, such as B, Al, and Ga, etc., to identify the zeolite structure with the highest acidity. Second, we use molecular dynamics (MD) to study the sorbate diffusion inside IM-12 zeolite. For the purpose of comparison, a unidirectional large-pore zeolite MOR with 12-MR is also considered. Especially, we selected the large molecules of diisopropylbenzene (DIPB) and triisopropylbenzene (TIPB), as probe molecules to study the reactance diffusion.

2. Methodology

In the work reported here, all the density functional theory (DFT) and molecular dynamics (MD) calculations were performed with the program package DMol^3 and Forcite in Materials Studio (version 3.1) of Accelrys Inc. [36]. The total energy optimization has been performed using the local density approximation (LDA) at Perdew–Wang (PWC) functional [37–39] and the generalized gradient approximation (GGA) at BLYP (the exchange correction of Becke and the correlation function of Lee, Yang, and Parr) functionals [40]. All electrons were included in the calculations. Double numerical basis set with polarization functions (DNP) has been used in all calculations carried out in this study. This basis set is comparable to 6-31G** set [41]: however, the numerical basis set is much better than the Gaussian basis set of the same size [37,42]. The energy convergence tolerance was set to 2.0×10^{-5} Ha, the maximum force 0.004 Ha/Å, and the maximum displacement 0.005 Å.

The IM-12 zeolite has 12 inequivalent tetrahedral (T) sites. The Ge atoms preferentially occupy T11 and T12 sites, which are those sites forming the double four-member rings (D4R) units [43–46]. Therefore, this is a new example in which Ge directs the synthesis towards zeolites that contain D4R units in their structures. The zeolite pore aperture

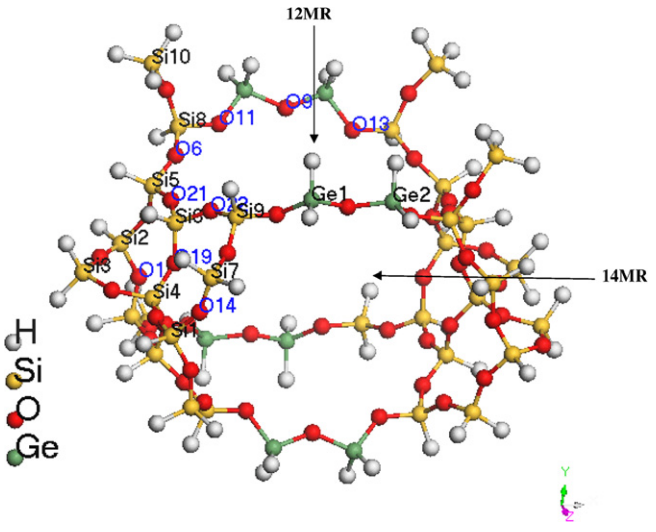

Fig. 1. Cluster model for IM-12 framework with 10 T sites.

was simulated by a T_{34} cluster (shown in Fig. 1) with 129 atoms, in which 25 atoms are Si, one Al atom, eight Ge atoms, 41 O atoms, and 54 H atoms which are located 1.46 Å from each of the Si atoms and oriented in the direction of what would normally be the next O atom. The geometry of the cluster models used in present study was taken from the crystal structure of IM-12 zeolite [11]. In the optimization, the outermost hydrogens were held fixed in their crystallographic position and the rest atoms were fully optimized. The crystallographic labeling of T sites IM-12 is in accordance with Atlas of Zeolite Framework Types [47].

In the MD simulation, we adopted the pure silica analogue of zeolites, to simplify the simulations [26,34,48,49]. The model of IM-12 and MOR, are constructed according to Ref. [50]. From the references, many types of force fields for zeolite are available, but it seems that many of them lack strict validations. So in the simulation of zeolite, it is very important to carefully choose the adequate force field. In this paper, the potential parameters are selected from the Dreiding, which has been fully validated by many works [51–54]. The Dreiding force fields, developed by Mayo et al. [54], is a good, all-purpose force field that can be used for structure predictions and dynamics calculations of organic, biological, and main-group inorganic molecules. The simulated zeolite system comprises a $2 \times 2 \times 2$ super cell with a total of 1824 and 1152 atoms for IM-12 and MOR, respectively, to which the periodic boundary condition is applied. The sorbate loadings were four molecules in the IM-12 super cell, which corresponds to 0.5 molecule/unit cell. The electrostatic interaction is evaluated through the Ewald sum method [55] and van der Waals interactions with a 12.5 Å cutoff. First, a run of 20 ps is performed to equilibrate the initial structures. Then an additional run of 1800 ps with a time step of 1 fs is carried out within a NVE (number of particles, N; volume, V; and energy, E are constant) microcanonical ensemble at 300 K. The history file from which data analysis of the diffusion process is carried out is saved every 5 ps and subsequently, the mean-square displacements (MSD) of the sorbate molecules can be calculated by

$$\langle X^2(t)\rangle = \frac{1}{N_m N_{t_0}} \sum_m \sum_{t_0} [X_i(t+t_0) - X_i(t_0)]^2 \quad (1)$$

where N_m is the number of diffusion molecules, N_{t_0} is the number of the time origins used in calculating the average, t_0 is the initial time, and X_i is the coordinate for the center of mass of molecule i.

3. Results and discussion

3.1. Density functional theory calculation

We optimized the clusters with Al substitutions on 10 inequivalent T sites in IM-12 zeolite. Two of the T sites embedded inside the zeolite framework are attributed to

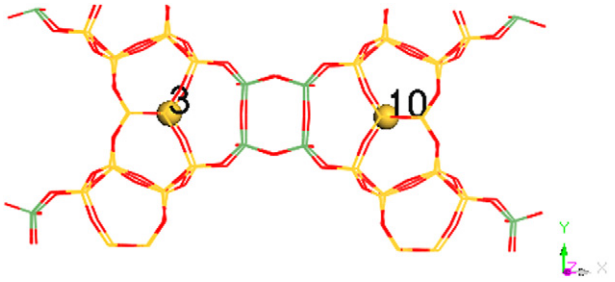

Fig. 2. The [0 0 1] projections of IM-12 showing the T3 and T10 sites.

T3 and T10 (see Fig. 2), which are inaccessible to the reactant molecules and excluded from our calculations. The similar approach has been used by Zhou et al. [56]. In this study, we report calculations on the substitution of silicon or germanium (for T11 and T12 sites) atoms by aluminums in the framework of cluster. A comparison of the substitution energy values for the T sites shows that the substitution energy value for T11 and T12 sites is about 40 times larger than that for the other T sites. The calculated substitution energies through the DFT-LDA and the DFT-GGA approximations for the rest eight inequivalent T sites are shown in Fig. 3. We can remark that trends between the LDA and GGA substitution energies are the same. In both cases, they indicate that the T4 and T6 sites are the most preferable locations for aluminum substitution. The deprotonation energies calculated within GGA are consistently bigger than those found through LDA calculations. According to crystallographic labeling of pure silica IM-12, all the T sites at the external surface pocket are T4 and T6 sites. There is a perfect match between NMR experiment and theoretical calculation [25,57], which concluded that the T sites located at the openings of the external surface pockets of the zeolite were the most preferable locations for aluminum substitution. Thus, the two sites have been selected to study acidities for various substitutions such as B and Ga, which have been used to alter catalytic activity, selectivity, and stability [58–61].

The acidities of substituted IM-12 zeolite can be evaluated by the reaction $ZOH \rightarrow ZO^- + H^+$, where ZO^- and

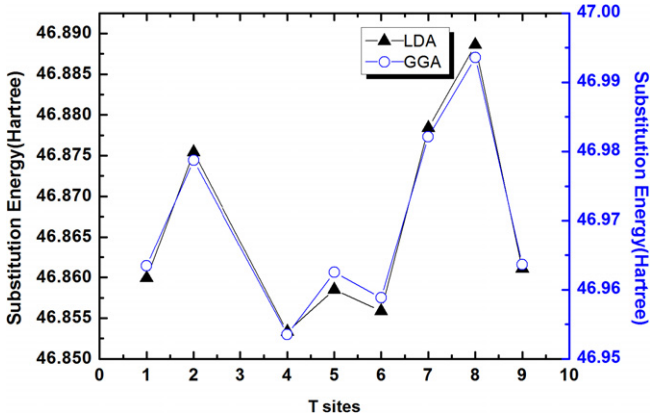

Fig. 3. The substitution energy on different sites, E (Al, Si) (kcal/mol).

ZOH represent the deprotonated and the neutral zeolites, respectively. The deprotonation energy (DPE) is the energy difference between deprotonated and neutral zeolite. Acid site with high deprotonation energy will be a poor proton donor and hence has a low Brönsted acidity. On the other hand, acid site having low deprotonation energy will act as good proton donors and hence show high Brönsted acidity. This rule indicates the acidities directly depend on the deprotonation energy of the deprotonation reaction.

When a Si atom was substituted by an Al atom in zeolite systems, the proton could be placed in all the four distinct oxygen atoms linked to the corresponding Al. Here, we calculated the deprotonation energy (DPE) of the protons located in the 14- or 12-membered ring as shown in Table 1. Based on the calculated deprotonation energy (DPE) values, we can conclude that the T4–O19–Si6 and T6–O21–Si5 sites show higher Brönsted acidity than other sites. It is worth noting that the T5–O21–Si6 also has the relative lower deprotonation energy (see Table 1), while the substitution at the T5 site is less favored energetically. These results confirm us to choose the two sites in the latter study (notated as M-T4 and M-T6, respectively).

The M–T4 and M–T6 clusters consisted of T = Si, B, Al, and Ga atoms were optimized using spin-restricted procedures. We performed density functional theory (DFT) calculations using both the local density approximation (LDA) and the generalized gradient approximation (GGA). Table 2 summarizes the calculated deprotonation energy (DPE) and the adsorption energies (E_{ads}) for NH_3 molecules of various isomorphous substitutions. The analysis of Table 2 shows that LDA and GGA give the same trends of the deprotonation energy (DPE). On the basis of the deprotonation energy, we can get the relative acidic order of the substituted IM-12 is: B–IM-12 < Ga–IM-12 < Al–IM-12. The acidity orders derived from deprotonation energy (DPE) index for characterizing the relative acidity of M–IM-12 are the same as other zeolites [62–64].

The NH_3 adsorption energy (E_{ads}) is another criterion for estimating the relative acidity of M–IM-12. It should be mentioned that the adsorption energy of NH_3 has been used carefully to measure and to predict the acidic properties of many zeolites [65–68]. The adsorption energy of ammonia was calculated according to the following equation:

$$E_{ads} = E - E_{ZeOH\text{-}NH_3} - E_{ZeOH} - E_{NH_3}$$

where the species ZeOH–NH_3 corresponds to the partially optimized ZeOH–NH_3 cluster, Z–OH and NH_3, respectively, correspond to the isolated partially optimized ZeOH clusters and the fully optimized NH_3 molecule. As we known, the higher adsorption energy indicates that the Brönsted acidity is stronger. From the Table 2, we can clearly see that the relative acidic order of M–IM-12 zeolite is B < Ga < Al. It agrees well with the order from the deprotonation energy. It should also be noted that the adsorption energies of NH_3 in H–[Al]MOR zeolite is presented [66,69]. Based on the adsorption energies of NH_3, the acid strength of H–[Al]IM-12 is comparable with that of H–[Al]MOR. Some studies have reported that the Ge in the double four-member rings (D4R) units have an effect on the acidity of zeolites [70,71]. To the best of our knowledge, there are no reports in the isomorphous substitution zeolites which is the Ge in the double four-member rings (D4R) units. In spite of this, more experimental and theoretical studies are necessary to be carried out on the isomorphous substitution IM-12 zeolite.

Table 1
Values for the deprotonation energy (DPE) (kcal/mol) and the relative deprotonation energy (E_{rel}) (kJ/mol) calculated by different methods

Proton points to		LDA		GGA	
		DPE	E_{rel}	DPE	E_{rel}
T1-O14-Si7	14-MR	290.96	4.85	298.06	9.00
T2-O1-Si5	14-MR	290.53	3.05	296.54	2.64
T4-O19-Si6	14-MR	289.80	0	296.19	1.17
T5–O1–Si2	14-MR	291.11	5.48	297.81	7.95
T5–O21–Si6	12-MR	290.90	4.60	296.07	0.67
T5–O6–Si8	12-MR	292.89	12.93	298.39	10.38
T6–O19–Si4	14-MR	291.17	5.73	297.19	5.36
T6–O21–Si5	12-MR	290.33	2.21	295.91	0
T6–O22–Si9	12-MR	291.74	8.12	297.51	6.70
T7–O14–Si1	14-MR	292.51	11.34	299.32	14.27
T8–O6–Si5	12-MR	295.33	23.14	301.32	22.64
T8–O11–Ge	12-MR	307.62	74.56	314.18	76.44
T9–O13–Ge	12-MR	301.20	47.70	307.30	47.66

Table 2
Deprotonation energy (DPE) (kcal/mol), and adsorption energy E_{ads} (kcal/mol) of NH_3 on the acid sites in the substitution IM-12 based on M-T4 and M-T6 clusters

Metal	M-T4		M-T6	
	DPE	E_{ads}	DPE	E_{ads}
LDA				
B	299.62	−38.50	301.34	−40.24
Al	289.80	−49.81	290.33	−51.14
Ga	295.24	−47.69	297.46	−49.65
GGA				
B	309.38	−19.85	309.55	−19.56
Al	296.19	−34.91	297.51	−36.79
Ga	302.02	−32.42	303.34	−33.72
Al (Calculated)[a]		−35.35 [64]		
Al (Experimental)[a]		−38.20 [68]		

[a] The calculated and experimental E_{ads} of NH_3 in H–[Al]MOR, respectively.

3.2. Molecular dynamics simulations

The study of the diffusion of sorbates through the channel systems of zeolites has become increasingly important owing to the need to obtain a better understanding of the mechanisms of catalysis and adsorption in these materials. IM-12, as one of the first microporous materials with two-dimensional channel systems of 14- and 12-membered rings (MR), has the potential to be acid catalysts for large molecules. Two molecules with different sizes, i.e., diisopropylbenzene (DIPB) and triisopropylbenzene (TIPB) have been

used as probe molecules to study the diffusion kinetics of large molecules inside IM-12. We also selected MOR as comparison. There are two reasons for adopting MOR as comparison: (1) one aim of this work is to estimate the influence of the channel (12- and 14-MR) system of the zeolites on the diffusion of sorbates. Among many zeolites, MOR is a particular useful catalyst for several applications and represents an interesting structure, for it is a high-silica zeolite which contains the two-dimensional channel system with large-pore 12-channels connected by alternating 8-channels. This can be compared with IM-12 that contains the two-dimensional channel system with extra-large-pores by 12- and 14-channels; (2) although MOR has quite big size unit cell containing 144 ions, it is relatively smaller than other large-pore zeolites. This can save the computational cost.

From the trajectory file, we calculated the mean-square displacements (MSD) in the Fig. 4, which shows the MSD plot for DIPB and TIPB in the IM-12 and MOR zeolite, respectively. From the slop of the MSD line, we obtained the diffusion coefficients D, by means of the Einstein relationship [72]

$$\langle X^2(t)\rangle = 6Dt + B \tag{2}$$

where t is the simulation time and B is the thermal factor arising from atomic vibrations. The diffusion coefficients obtained from MSD plot are listed in Table 3. With the same force field, charges, and calculation conditions, the coefficients D in the IM-12 are larger than the situations in MOR for DIPB and TIPB, respectively. As shown in Table 3, DIPB molecule can easily penetrate both the zeolite with large-pore (MOR) and extra-pores (IM-12). Another type of probe molecule (TIPB), which is too large to be easily adsorbed into the large-pore of MOR but, at the same time, is sufficiently small to access extra-pores (IM-12). Also note that its TIPB adsorption capacity is larger than the DIPB adsorption capacities in the zeolite IM-12 and MOR. The diffusion behavior of the molecules is in correspondence with the previous experimental study [2], in

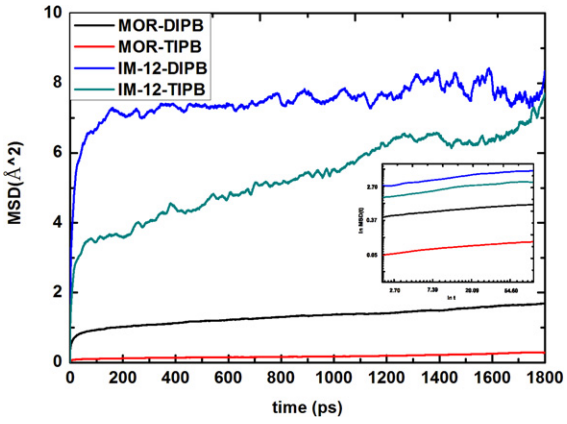

Fig. 4. Mean-square displacements (MSD) for the 1800 ps runs of DIPB and TIPB in the MOR and IM-12, respectively. Insets show a ln–ln plot of the same curves.

Table 3
Diffusion coefficients of DIPB and TIPB obtained from the MSD plots in Fig. 4

Zeolite	Diffusion coefficient (cm^2/s)	
	DIPB	TIPB
MOR	1.78×10^{-6}	0.40×10^{-6}
IM-12	3.03×10^{-6}	8.83×10^{-6}

which the kinetic rate constants for dealkylation of TIPB is higher than DIPB in ITQ-15. These results indicate that the effective size and shape of the pore openings in these 14- and 12-membered ring zeolites become critical to the diffusion of TIPB molecules [2] and the two-dimensional channel system with extra-large-pores by 14- and 12-channels in UTL (IM-12 and ITQ-15) may have significant selectivity for TIPB over DIPB. Adsorption of TIPB may discriminate the dimensions of 12- and 14-membered ring pore zeolites, which is consistent with other report [73]. This behavior can be attributed to the restriction of the diffusion of guest molecules by the size of the zeolite crystals and indicates the catalytic benefit of the two-dimensional channel system of IM-12 with respect to the two-dimensional pore topology in the case of MOR. On the basis of comparison of the adsorption results in IM-12 for DIPB and TIPB with those of the MOR zeolite in Table 3, IM-12 appears to have the pore benefit of the diffusion of large molecules, especially for the bulky molecule TIPB.

4. Conclusions

We have carried out DFT and MD simulations to study the acid and dynamics behavior for IM-12 zeolite. In both LDA and GGA approaches, it was shown that the sites T4 and T6 are the two preferable sites to replace with Al substitutions. Isomorphously substituting gives the Brönsted acidity order: B–IM-12 < Ga–IM-12 < Al–IM-12, which is the same as other zeolites. Based on the adsorption energies of NH_3, the acid strength of H–[Al]IM-12 is comparable with that of H–[Al]MOR. The diffusion coefficient obtained from the MD indicated the catalytic benefit of the two-dimensional channel system of IM-12 with respect to the MOR and IM-12 may have significant selectivity for TIPB over DIPB. In summary, we found that IM-12 is a good candidate as the acidity catalysts for large molecules such as DIPB and TIPB, superior to the large-pore zeolite (MOR).

Acknowledgments

This research was supported by NKBRSF (2006CB815202). K.L.H. is a member of Virtual Laboratory for Computational Chemistry, CNIC, CAS.

References

[1] M.E. Davis, C. Saldarriaga, C. Montes, J. Garces, C. Crowder, Nature 331 (1988) 698.

[2] A. Corma, M.J. Díaz-Cabañas, F. Rey, S. Nicolopoulus, K. Boulahya, Chem. Commun. 12 (2004) 1356.
[3] C.C. Freyhardt, M. Tsapatsis, R.F. Lobo, K.J. Balkus, M.E. Davis, Nature 381 (1996) 295.
[4] R.F. Lobo, M. Tsapatsis, C.C. Freyhardt, S. Khodabandeh, P. Wagner, C.Y. Chen, K.J. Balkus, S.I. Zones, M.E. Davis, J. Am. Chem. Soc. 119 (1997) 474.
[5] P. Wagner, M. Yoshikawa, M. Lovallo, K. Tsuji, M. Tsapatsis, M.E. Davis, Chem. Commun. 22 (1997) 2179.
[6] K.G. Strohmaier, D.E.W. Vaughan, J. Am. Chem. Soc. 125 (2003) 16035.
[7] A. Burton, S. Elomari, C.Y. Chen, R.C. Medrud, I.Y. Chan, L.M. Bull, C. Kibby, T.V. Harris, S.I. Zones, E.S. Vittoratos, Chem. Eur. J. 9 (2003) 5737.
[8] T. Cheetham, H. Fjellvag, T.E. Gier, K.O. Kongshaug, K.P. Lillerud, G.D. Stucky, Stud. Surf. Sci. Catal. 135 (2001) 788.
[9] A. Corma, M.J. Díaz-Cabañas, J.L. Jordá, C. Martínez, M. Moliner, Nature 443 (2006) 842.
[10] J. Martinez-Triguero, M.J. Diaz-Cabanas, M.A. Camblor, V. Fornes, Th.L.M. Maesen, A. Corma, J. Catal. 182 (1999) 463.
[11] J.L. Paillaud, B. Harbuzaru, J. Patarin, N. Bats, Science 304 (2004) 990.
[12] J. Limtrakul, D. Tantanak, Chem. Phys. 208 (1996) 331.
[13] S.L. Suib, Chem. Rev. 93 (1993) 803.
[14] P. Kortunov, S. Vasenkov, J. Kärger, M.F. Elia, M. Perez, M. Stöcker, G.K. Papadopoulos, D. Theodorou, B. Drescher, G. McElhiney, B. Bernauer, V. Krystl, M. Kocirik, A. Zikanova, H. Jirglova, C. Berger, R. Gläser, J. Weitkamp, E.W. Hansen, Chem. Mater. 17 (2005) 2466.
[15] S. Gomez, O. Giraldo, L.J. Garces, J. Villegas, S.L. Suib, Chem. Mater. 16 (2004) 2411.
[16] S. Gomez, L.J. Garces, J. Villegas, R. Ghosh, O. Giraldo, S.L. Suib, J. Catal. 233 (2005) 60.
[17] B.O. Hincapie, L.J. Garces, S. Gomez, R. Ghosh, S.L. Suib, Catal. Today 110 (2005) 323.
[18] J. Luo, Q.H. Zhang, A.M. Huang, S.L. Suib, Micropor. Mesopor. Mater. 36 (2000) 209.
[19] H.B. Mostad, M. Stoecker, A. Karlsson, T. Rørvik, Appl. Catal. A 144 (1996) 305.
[20] M. Niwa, S. Nishikawa, N. Katada, Micropor. Mesopor. Mater. 82 (2005) 105.
[21] A.R. Ruiz-Salvador, D.W. Lewis, J. Rubayo-Soneira, G. Rodriguez-Fuentes, L.R. Sierra, C.R.A. Catlow, J. Phys. Chem. B 102 (1998) 8417.
[22] P. Viruela-Martin, C.M. Zicovich-Wilson, A. Corma, J. Phys. Chem. 97 (1993) 13713.
[23] P. Strodel, K.M. Neyman, H. Knözinger, N. Rösch, Chem. Phys. Lett. 240 (1995) 547.
[24] M.S. Stave, J.B. Nicholas, J. Phys. Chem. 99 (1995) 15046.
[25] Y. Wang, J.Q. Zhuang, G. Yang, D.H. Zhou, D. Ma, X.W. Han, X.H. Bao, J. Phys. Chem. B 108 (2004) 1386.
[26] T.J. Hou, L.L. Zhu, X.J. Xu, J. Phys. Chem. B 104 (2000) 9356.
[27] H. Paoli, A. Méthivier, H. Jobic, C. Krause, H. Pfeifer, F. Stallmach, J. Kärger, Micropor. Mesopor. Mater. 55 (2002) 147.
[28] H. Jobic, H. Ernst, W. Heink, J. Kärger, A. Tuel, M. Bée, Micropor. Mesopor. Mater. 26 (1998) 67.
[29] P. Kortunov, S. Vasenkov, J. Karger, R. Valiullin, P. Gottschalk, M. Fe Elia, M. Perez, M. Stocker, B. Drescher, G. McElhiney, C. Berger, R. Glaser, J. Weitkamp, J. Am. Chem. Soc. 127 (2005) 13055.
[30] L. Gjerdaker, D.W. Aksnes, G.H. Sorland, M. Stocker, Micropor. Mesopor. Mater. 42 (2001) 89.
[31] F. Courivaud, E.W. Hansen, S. Kolboe, A. Karlsson, M. Stöcker, Micropor. Mesopor. Mater. 37 (2000) 223.
[32] F. Courivaud, E.W. Hansen, A. Karlsson, S. Kolboe, M. Stöcker, Micropor. Mesopor. Mater. 35 (2000) 327.
[33] A. Sayeed, S. Mitra, A.V.A. Kumar, R. Mukhopadhyay, S. Yashonath, S.L. Chaplot, J. Phys. Chem. B 107 (2003) 527.
[34] G. Sastre, A. Corma, C.R.A. Catlow, Top. Catal. 9 (1999) 215.
[35] S. Al-Khattaf, H.I. de Lasa, Appl. Catal. A 226 (2002) 139.
[36] DMol^3, version 3.1 from Accelrys: <http://www.accelrys.com/mstudio/dmol3.html>.
[37] B. Delley, J. Chem. Phys. 92 (1990) 508.
[38] B. Delley, J. Phys. Chem. 100 (1996) 6107.
[39] B. Delley, J. Chem. Phys. 113 (2000) 7756.
[40] A.D. Becke, Phys. Rev. A 38 (1998) 3098.
[41] W.J. Hehre, L. Radom, P.R. Schleyer, J.A. Pople, Ab Initio Molecular Orbital Theory, Wiley, New York, 1986.
[42] B. Delly, Phys. Rev. B 65 (2002) 085403.
[43] G. Sastre, A. Pulido, A. Corma, Chem. Commun. 18 (2005) 2357.
[44] T. Blasco, A. Corma, M.J. Diaz-Cabanas, F. Rey, J.A. Vidal-Moya, C.M. Zicovich-Wilson, J. Phys. Chem. B 106 (2002) 2634.
[45] G. Sastre, A. Pulido, A. Corma, Micropor. Mesopor. Mater. 82 (2005) 159.
[46] M.A. Zwijnenburg, S.T. Bromley, J.C. Jansen, T. Maschmeyer, Micropor. Mesopor. Mater. 73 (2004) 171.
[47] W.M. Meier, D.H. Olson, C. Baerlocher, Atlas of Zeolite Structure Types, fourth ed., Elsevier, Amsterdam, 1996. <http://ww.iza-structure.org/databases/>.
[48] G. Sastre, N. Raj, C.R.A. Catlow, R. Roque-Malherbe, A. Corma, J. Phys. Chem. B 102 (1998) 3198.
[49] G. De Luca, P. Pullumbi, G. Barbieri, A.D. Fama, P. Bernardo, E. Drioli, Sep. Purif. Technol. 36 (2004) 215.
[50] C. Baerlocher, W.M. Meier, D.H. Olson, Atlas of Zeolite Framework Types, fifth ed., Elsevier, Amsterdam, 2001.
[51] J.X. Liu, M. Dong, Z.F. Qin, J.G. Wang, J. Mole. Struct. (Theochem.) 679 (2004) 95.
[52] E. Klemm, J.G. Wang, G. Emig, Micropor. Mesopor. Mater. 26 (1998) 11.
[53] J.R. Fried, S. Weaver, Comp. Mater. Sci. 11 (1998) 277.
[54] S.L. Mayo, B.D. Olafson, W.A. Goddard, J. Phys. Chem. 94 (1990) 8897.
[55] P.P. Ewald, Ann. Physik 64 (1921) 253.
[56] D.H. Zhou, Y. Bao, M.M. Yang, N. He, G. Yang, J. Mol. Catal. A 244 (2006) 11.
[57] D.H. Zhou, Y. Wang, D. Ma, X.H. Bao, Chem. J. Chin. Univ. 27 (2002) 207.
[58] A. Chatterjee, T. Iwasaki, T. Ebina, A. Miyamoto, Micropor. Mesopor. Mater. 21 (1998) 421.
[59] S.P. Yuan, J.G. Wang, Y.W. Li, H.J. Jiao, J. Phys. Chem. A 106 (2002) 8167.
[60] A. Kyrlidis, S.J. Cook, A.K. Chakraborty, A.T. Bell, D.N. Theodorou, J. Phys. Chem. 99 (1995) 1505.
[61] S.P. Yuan, J.G. Wang, Y.W. Li, S.Y. Peng, J. Mol. Catal. A 178 (2002) 267.
[62] Y. Yokomori, J. Wachsmuth, K. Nishi, Micropor. Mesopor. Mater. 50 (2001) 137.
[63] A. Redondo, P.J. Hay, J. Phys. Chem. 97 (1993) 11754.
[64] C. Lo, B.L. Trout, J. Catal. 227 (2004) 77.
[65] M. Elanany, M. Koyama, M. Kubo, P. Selvam, A. Miyamoto, Micropor. Mesopor. Mater. 71 (2004) 51.
[66] M. Elanany, D.P. Vercauteren, M. Koyama, M. Kubo, P. Selvam, E. Broclawik, A. Miyamoto, J. Mol. Catal. A 243 (2006) 1.
[67] M. Elanany, D.P. Vercauteren, M. Kubo, A. Miyamoto, J. Mol. Catal. A 248 (2006) 181.
[68] M. Elanany, B.L. Su, D.P. Vercauteren, J. Mol. Catal. A 263 (2006) 195.
[69] C. Lee, D.J. Parrillo, R.J. Gorte, W.E. Farneth, J. Am. Chem. Soc. 118 (1996) 3262.
[70] L.G.A. van de Water, M.A. Zwijnenburg, W.G. Sloof, J.C. van der Waal, J.C. Jansen, T. Maschmeyer, Chem. Phys. Chem. 5 (2004) 1328.
[71] C.M. Zicovich-Wilson, A. Corma, J. Phys. Chem. B 104 (2000) 4134.
[72] A. Einstein, Ann. Phys. (Leipzig) 17 (1905) 549.
[73] A. Burton, S. Elomari, R.C. Medrud, I.Y. Chan, C.Y. Chen, L.M. Bull, E.S. Vittoratos, J. Am. Chem. Soc. 125 (2003) 1633.